Liquid Crystals
Publication details, including instructions for authors and subscription information:
http://www.informaworld.com/smpp/title~content=t713926090

Blue phases and twist grain boundary phases (TGBA and TGBC) in a series of fluoro-substituted chiral tolane derivatives

Min-Hui Li; Valerie Laux; Huu-Tinh Nguyen; Gilles Sigaud; Philippe Barois; Noel Isaert

Online publication date: 29 June 2010

To cite this Article Li, Min-Hui , Laux, Valerie , Nguyen, Huu-Tinh , Sigaud, Gilles , Barois, Philippe and Isaert, Noel(1997) 'Blue phases and twist grain boundary phases (TGBA and TGBC) in a series of fluoro-substituted chiral tolane derivatives', Liquid Crystals, 23: 3, 389 — 408
To link to this Article: DOI: 10.1080/026782997208325
URL: http://dx.doi.org/10.1080/026782997208325

LIQUID CRYSTALS, 1997, VOL. 23, NO. 3, 389–408

Blue phases and twist grain boundary phases (TGBA and TGBC) in a series of fluoro-substituted chiral tolane derivatives

by MIN-HUI LI*, VALERIE LAUX†, HUU-TINH NGUYEN, GILLES SIGAUD, PHILIPPE BAROIS and NOEL ISAERT†

Centre de Recherche Paul Pascal, CNRS/Université de Bordeaux I, Avenue A. Schweitzer, 33600 Pessac Cedex, France

† Laboratoire de Dynamique et Structure des Matériaux Moléculaires, CNRS/ Université de Lille I, U.F.R. de Physique, 59655 Villeneuve d'Ascq Cedex, France

(*Received 12 February 1997; accepted 21 March 1997*)

A series of fluoro-substituted tolane derivatives: (*R*)-1-methylheptyl 3′-fluoro-4′-(3-fluoro-4-*n*-alkoxybenzoyloxy)tolane-4-carboxylates is reported. Some members of this series exhibit the phase sequence: Cr–SmC*–TGBC–TGBA–BPI–BPII–BPIII–I. The blue phases, the TGBA and TGBC phases and the SmC* phase were characterized in detail by microscopic observation, differential scanning calorimetry, helical pitch measurements, X-ray structural analysis and electro-optical study. The blue phases directly next to the TGBA phase were shown to be a new type of blue phase exhibiting smectic ordering. A commensurate TGBC phase with constant number of slabs per pitch was observed.

1. Introduction

The twist grain boundary (TGB) phases and the blue phases (BPs) are two kinds of frustrated phases of chiral molecules, resulting from the competition between the chiral forces and the desire for molecules to pack in ways such that they fill space uniformly.

The existence of a twist grain boundary smectic A (TGBA) phase in chiral systems was predicted by Renn and Lubensky in 1988 [1] based on the De Gennes model [2] and first demonstrated experimentally by Goodby *et al.* in 1989 [3, 4]. Theoretical work [1] proposed that the TGBA phase structure involved slabs of SmA material regularly stacked in a helical fashion along an axis parallel to the smectic layers. Adjacent slabs were continuously connected via a grain boundary which consisted of a grid of parallel equispaced screw dislocation lines. This periodic ordering of screw dislocations relieves the frustration for the molecules which need to form a helical structure. Renn and Lubensky also proposed the structure of tilted twist grain boundary TGBC and TGBC* phases in which the smectic slabs are, respectively, SmC and SmC* [5, 6]. The existence of the TGBC phase was demonstrated by the work of the Bordeaux group [7]. However, evidence for a structure different from that of the RL model was obtained, where the smectic layers are tilted relative to the pitch axis, while the molecular director remains perpendicular to the pitch axis [8, 9].

Blue phases exist in the first discovered liquid crystalline material (cholesteryl benzoate) [10], whereas the recognition of them as distinct thermodynamically stable phases was not made until the 1970s [11]. Theoretical and experimental work has demonstrated that cholesteric liquid crystals of short pitch can form up to three distinct blue phases [12–14] at the transition from cholesteric phase (N*) to the isotropic phase (I). In order of increasing temperature they are named blue phase I (BPI), blue phase II (BPII) and blue phase III (BPIII). BPI and BPII are cubic phases and have, respectively, body-centred cubic and simple cubic symmetry. BPIII is seemingly amorphous with a still unknown local structure. In the cubic blue phases, the basic unit is thought to be the double twist tube: a cylinder of liquid crystal material in which the director is parallel to the axis at the centre and rotates spatially about any radius. The double twist tube has been shown theoretically‡ to be more stable than the single twist structure of the N* phase at a higher temperature, when the chirality of the molecules is high enough such that the helical pitch is sufficiently short. Fitting these double twist cylinders into a three-dimensional structure so that the directors match everywhere is topologically impossible. Therefore disclinations, defects in the orientational arrangement of molecules, are necessary to relieve the

*Author for correspondence.

‡ The double twist tube has only been observed experimentally in lyotropic systems in the blue phases of concentrated DNA solutions, using freeze-fracture electron microscopy [15].

0267–8292/97 $12·00

elastic strain energy. The cubic blue phases can therefore be described as lattices of double twist tubes or, equivalently, lattices of defects.

Blue phases are normally found between the isotropic liquid state and a cholesteric phase of sufficiently short pitch in the phase sequence I–BPs–N*, except in two cases where a direct BPI–SmA transition has been observed [16, 17]. The twist grain boundary phases are typically detected at the phase transition from the isotropic liquid or cholesteric states to smectic states in the following sequences: I–**TGBA**–SmC*, I–BP–N*–**TGBA**–SmA, I–BP–N*–**TGBA**–SmC*, I–BP–N*–**TGBA**–**TGBC**–SmC* and I–BP–N*–**TGBC**–SmC*. Recently, we have reported the observation of a new phase sequence **I–BPs–TGBA** in a chiral tolane derivative [18], where the blue phases are observed for the first time between the isotropic state and the TGBA phase in the absence of a cholesteric phase. This sequence is also new from the point of view of the TGBA phase. This chiral material is (*R*) or (*S*)-1-methylheptyl 3′-fluoro-4′-(3-fluoro-4-octadecyloxybenzoyloxy)tolane-4-carboxylate (simply named FH/FH/HH-18BTMHC), whose chemical structure is shown below. We report now the detailed investigations of all members of this series (FH/FH/HH-*n*BTMHC) with different chain lengths ($n=7$–20). In the following sections, we will describe the synthesis (§2), the mesomorphic properties (§3), the helical pitch measurements (§4), the X-ray structural analyses (§5) and the electro-optical studies (§6). A summary will be given at the end.

2. Synthesis

The compounds FH/FH/HH-*n*BTMHC ($n=7$, 8, 9, 10, 11, 12, 13, 14, 16, 18, 20) were prepared according to scheme 1. Details of the syntheses are reported below. The synthesis of the substituted benzoic acids **8**, used in the final esterification step f, has been described elsewhere [19, 20]. The following examples are typical of the methods used to obtain the compounds indicated in the scheme. The infrared spectra were recorded on a Perkin-Elmer 783 spectrophotometer and the NMR spectra on a Bruker HW200 MHz spectrometer.

2.1. *1-Bromo-3-fluoro-4-tetrahydropyranyloxy benzene* (**2**)

To a stirred solution of 2-fluoro-4-bromophenol **1** (15·5 g; 81·2 mmol) in dichloromethane (50 ml, stabilized by 2-methyl-2-butene) cooled in an ice bath, dihydropyran (DHP) (8·27 g; 98·4 mmol) was added dropwise over 10 min. Some crystals of *p*-toluenesulphonic acid (PTSA) were then added. The reaction was complete after about 15 min (TLC showed no starting material remaining). The reaction was quenched by addition of $NaHCO_3$ (0·6 g). The solvent was removed by rotary evaporation and the liquid product was filtered through basic alumium oxide using heptane/ethyl acetate (9/1) mixture as eluent. The product (**2**) was a colourless oil. Yield: 20·7 g (93%). ^{1}H NMR ($CDCl_3$): 1·5–2·1 (m, 6H, 3$\underline{CH_2}$), 3·56–3·96 (m, 2H; $\underline{CH_2}$–O), 5·74 (t, 1H, $\underline{CH}$–O), 7·1–7·25 (m, 3H, arom.).

2.2. *3-Fluoro-4-tetrahydropyranyloxyphenylacetylene* (**4**)

Palladium(II) chloride ($PdCl_2$) (0·183 g, 1·03 mmol) and copper(II) acetate monohydrate ($Cu(AcO)_2 \cdot H_2O$ (0·199 g, 1·0 mmol) were added successively to a stirred solution of compound **2** (20 g, 73·0 mmol) and triphenylphosphine (TPP) (1·66 g, 6·34 mmol) in dipropylamine (*n*-Pr_2NH) (200 ml) under nitrogen. Then trimethylsilylacetylene (TMS) (8·7 g, 88·6 mmol) was added dropwise. The solution was gradually heated with an oil bath (106°C) and stirred for 4 h [21]. The stirred mixture was cooled to room temperature and the salt formed by the reaction was filtered off and washed well with heptane. The solvent in the filtrate was evaporated off in vacuum. The residue was hydrolysed with concentrated hydrochloric acid (16 ml), water (160 ml) and crushed ice (80 g). Organic materials were extracted into heptane (2 × 300 ml) and the organic phase was washed with water (250 ml), dried over anhydrous Na_2SO_4, filtered and evaporated. The residue was filtered through neutral alumium oxide using an heptane/ethyl acetate mixture (9/1). The solvent was removed on a rotary evaporator and the compound **3** so obtained (13·5 g, 46·2 mmol) was dissolved in tetrahydrofuran (THF) (20 ml) and methanol (20 ml). To this solution cooled in an ice bath was added dropwise with stirring a 50 per cent NaOH solution (4·6 g). The mixture was stirred at room temperature for 1 h. Heptane (120 ml) and water (120 ml) were then added. The organic phase was separated and washed with water (100 ml), dried over Na_2SO_4, filtered and evaporated. The compound **4** obtained was a reddish liquid. Yield: 10 g (64%). ^{1}H NMR ($CDCl_3$): 1·5–2·1 (m, 6H, 3$\underline{CH_2}$), 3·02 (s, 1H, $\underline{H}$–C≡C), 3·56–3·96 (m, 2H, $\underline{CH_2}$–O), 5·47 (t, $J=3$ Hz, 1H, $\underline{CH}$–O), 7·1–7·25 (m, 3H, arom.).

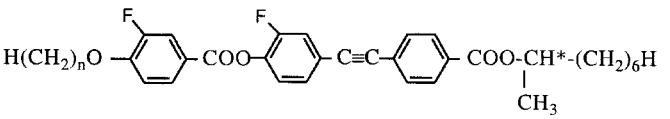

($n=18$)

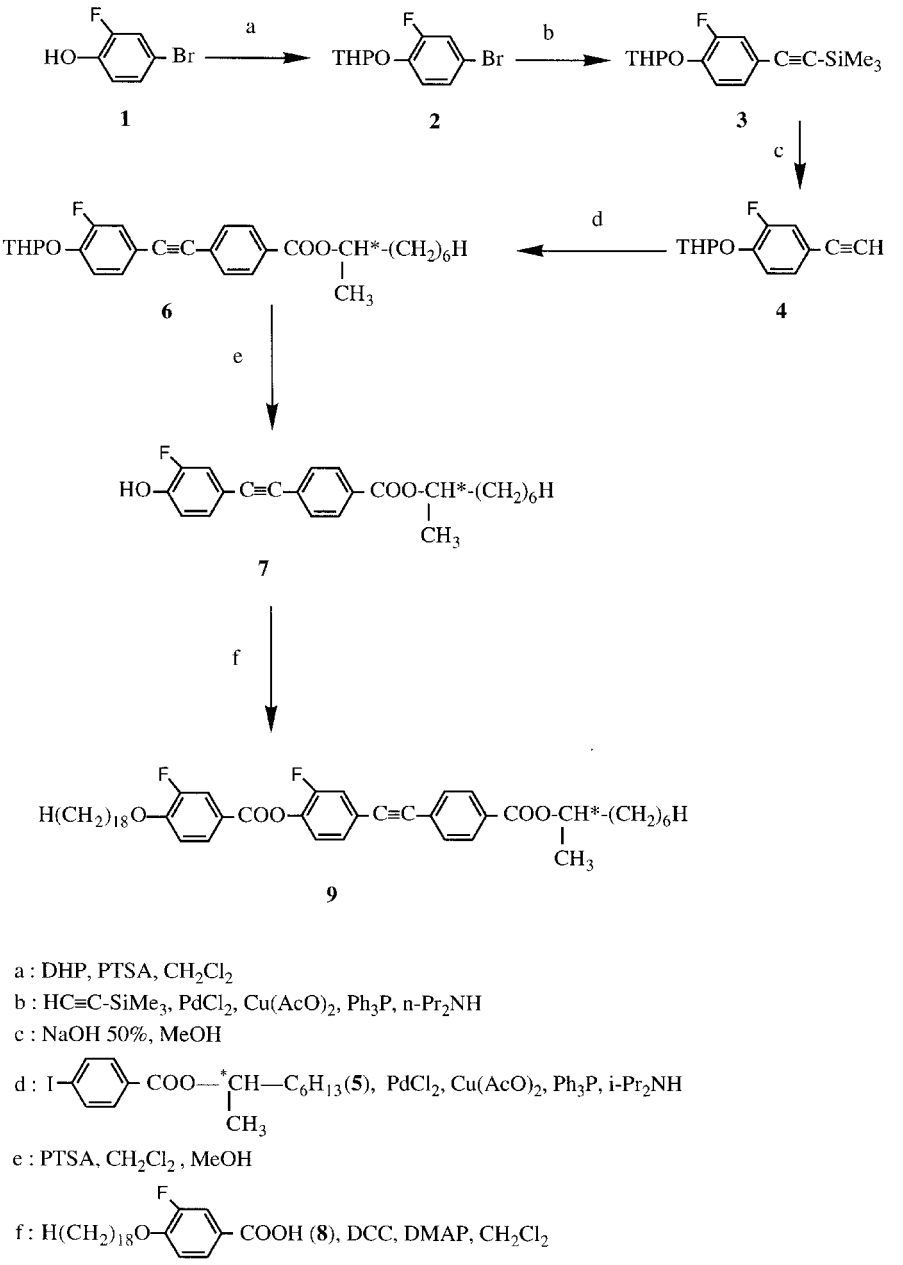

Scheme 1.

2.3. *(R) and (S)-1-Methylheptyl 4-iodobenzoate* (**5**) *and* (**5′**)

To a solution of (*R*)-2-octanol (5·2 g, 40 mmol) in CH_2Cl_2 (250 ml) was added dicyclohexylcarbodiimide (DCC) (8·1 g, 44 mmol), 4-dimethylaminopyridine (DMAP) (0·4 g, 3·3 mmol) and 4-iodobenzoic acid (9·92, 40 mmol). The mixture was stirred at room temperature overnight; the solution was then filtered and evaporated. The residue was purified by chromatography on silica gel using toluene as eluent. The compound **5** obtained was a slightly yellow liquid. Yield: 11·5 g (80%).

The (*S*)-1-methylheptyl 4-iodobenzoate **5′** was obtained by the Mitsunobu reaction [22]. To an ice cooled solution of 4-iodobenzoic acid (9·92 g, 40 mmol), (*R*)-2-octanol (5·72 g, 44 mmol) and triphenylphosphine (Ph_3P) (11·53 g, 44 mmol) in CH_2Cl_2 (80 ml) was added dropwise diethyl azodicarboxylate (DEAD) (7·66 g, 44 mmol). The mixture was stirred at room temperature for 2 h, it was then filtered and evaporated. Chromatography on silica gel with toluene as eluent was used to purify the product. Yield: 7·5 g (52%).

^{1}H NMR ($CDCl_3$): 0·84 (t, 3H, CH_2–$\underline{CH_3}$), 1·2–1·8 (m, 13H, aliphatic), 5·05–5·15 (m, 1H, O$\underline{CH}$(CH_3)CH_2),

7·7–7·8 (m, 4H, aromatic). IR (KBr) ν/cm^{-1}: 2930, 1720, 1590, 1390, 1280, 1270, 1110, 1100, 1010, 754.

2.4. *(R)-1-Methylheptyl 3′-fluoro-4′-hydroxytolane-4-carboxylate* (**7**)

A mixture of compound **4** (6·4 g, 28 mmol), compound **5** (11 g, 31 mmol), TPP (0·19 g, 0·73 mmol) and diisopropylamine (55 ml) was stirred under nitrogen and heated in an oil bath at 30°C until dissolution of solids was complete. The catalysts $PdCl_2$ (0·030 g, 0·17 mmol) and $(Cu(AcO)_2 \cdot H_2O)$ (0·030 g, 0·15 mmol) were added to this solution which was then gradually heated to 90°C and maintained at this temperature for 3 h. After cooling to room temperature the salt was removed by filtration and washed well with ethyl acetate. The filtrate was evaporated and the residue hydrolysed with concentrated hydrochloric acid (8 ml), water (80 ml) and crushed ice (40 g). The hydrolysate was then shaken with ethyl acetate. The organic phase was dried over Na_2SO_4, filtered and evaporated. The residue was filtered through neutral aluminium oxide using a heptane/ethyl acetate (95/5) mixture. The intermediate compound **6** (10·8 g, 23 mmol) so obtained was dissolved in a CH_2Cl_2 (70 ml) and CH_3OH (120 ml) mixture. To this solution was added PTSA (0·3 g) and the mixture was stirred at room temperature for 1 h. The solvent was evaporated and the pure phenol **7** obtained by chromatography on silica gel using heptane/ethyl acetate (8/2) mixture as eluent. The compound recrystallized in the refrigerator as a yellow solid. Yield: 8·4 g (78%). ^{1}H NMR ($CDCl_3$): 0·88 (t, J=6·4 Hz, 3H CH_2–$\underline{CH_3}$), 1·2–1·8 (m, 13H, 5$\underline{CH_2}$, CH–$\underline{CH_3}$), 5·16 (m(4t), J=6·4 Hz, 1H, $\underline{CH}$–CH_3), 5·65 (d, $^4J_{HF}$=4 Hz, $\underline{HO}$–Ph), 6·99 (t,J=8·8 Hz, 1H, arom. *ortho* to OH), 7·22–7·31 (m, 2H arom. *meta* to OH), 7·55 (d, 2H, arom. *ortho* to –C≡C–), 8·02 (d, 2H, arom. *ortho* to –COO). IR (KBr) ν/cm^{-1}: 3400 (Ph–OH), 2900 (C–H), 2210 (–C≡C–), 1690, 1620, 1600, 1280, 1110, 850.

2.5. *(R)-1-Methylheptyl 3′-fluoro-4′-(3-fluoro-4-octadecyloxybenzoyloxy) tolane-4-carboxylate* (**9**) *(n=18)*

To a solution of phenol **7** (0·192 g, 0·5 mmol) in CH_2Cl_2 (5 ml) was added DCC (0·101 g, 0·55 mmol), DMAP (0·010 g) and 3 fluoro-4-decyloxybenzoic acid **8**. The resulting mixture was stirred at room temperature overnight. The solution was filtered and evaporated. The residue was purified by chromatography on silica gel with toluene as eluent. The product (white powder) was crystallized from absolute ethanol. Yield: 0·28 g (74%). ^{1}H NMR ($CDCl_3$): 0·86 (t, 6H, 2$\underline{CH_3}$), 1·25 (m, 38H, 19$\underline{CH_2}$), 1·31 (d, 3H, $\underline{CH_3}$–CH), 1·8 (m, 4H, OCH$\underline{CH_2}$, O$CH_2\underline{CH_2}$), 4·11 (t, 2H, O$\underline{CH_2}$), 5·15 (m, 1H, $\underline{CH}CH_3$), 7·02 (t, 1H arom. *ortho* to OR), 7·2–8·0 (m, 9H arom.).

3. Mesomorphic properties

The mesomorphic properties of the derivatives obtained were studied by polarized optical microscopy and differential scanning calorimetry. We used a Leitz Ortholux microscope equipped with a Mettler FP5 hot stage for the optical observations and a Perkin-Elmer DSC7 for the calorimetric study. The contact method between two enantiomers was used and the racemic products were studied.

3.1. *TGBA–BPs–I phases*

When cooling at a slow rate from the isotropic phase, there is no evidence of blue phase textures up to n=14 in the series. For the n=14, 16 and 18 homologues, two blue phases have detectable textures. We observe first some blue–grey square-shaped single crystals of BPII growing very rapidly in the dark background. The growth ends by forming the typical BPII mosaic texture composed of platelets [18]. On further cooling, the characteristic cross-hatching resulting from the phase transition BPII→BPI [23] appears in the platelets. This paramorphotic texture of BPI persists only over a very narrow interval of temperature: 0·1°C for n=14, 0·4°C for n=16 and 0·2°C for n=18. Finally, in the compound n=20, BPII alone was observed on cooling. For all compounds the temperature of the transition to the TGBA phase is easily determined through the bright and coloured texture that develops with decreasing temperature (the assignment of the TGBA phase will be discussed below). If the samples of n=14, 16, and 18 are reheated, this bright and coloured texture vanishes, and a mosaic texture with smaller platelets is restored. No striation is visible for any of the three derivatives. In these cases, we think that BPII is obtained directly because of superheating of the TGBA phase.

The DSC thermograms of the compound n=18 on heating and on cooling at a temperature rate of 0·2°C min^{-1} are given in figure 1. The DSC thermograms of the homologues with n=14 and n=16 are similar to those of n=18. On cooling, we observe a large C_p variation 1 followed by three sharp peaks 2, 3 and 4 within ~5°C, while upon heating only two sharp peaks 2 and 3 are detected previous to the large C_p feature. Estimation of the enthalpies shows that the sum of ΔH_3 and ΔH_4 upon cooling is equivalent to ΔH_3 upon heating for the compounds with n=14, 16 and 18 (all results related to the DSC analysis, transition temperatures and enthalpies, are summarized in table 1). All these observations are consistent with the microscopic assignment of the BPI and BPII phases. The broad specific heat variation 1 could correspond to a I–BPIII transition [24]. However, by microscopic observation, no such fog phase (BPIII) could be detected. This is not so surprising considering that BPIII shows only a faint blue or grey

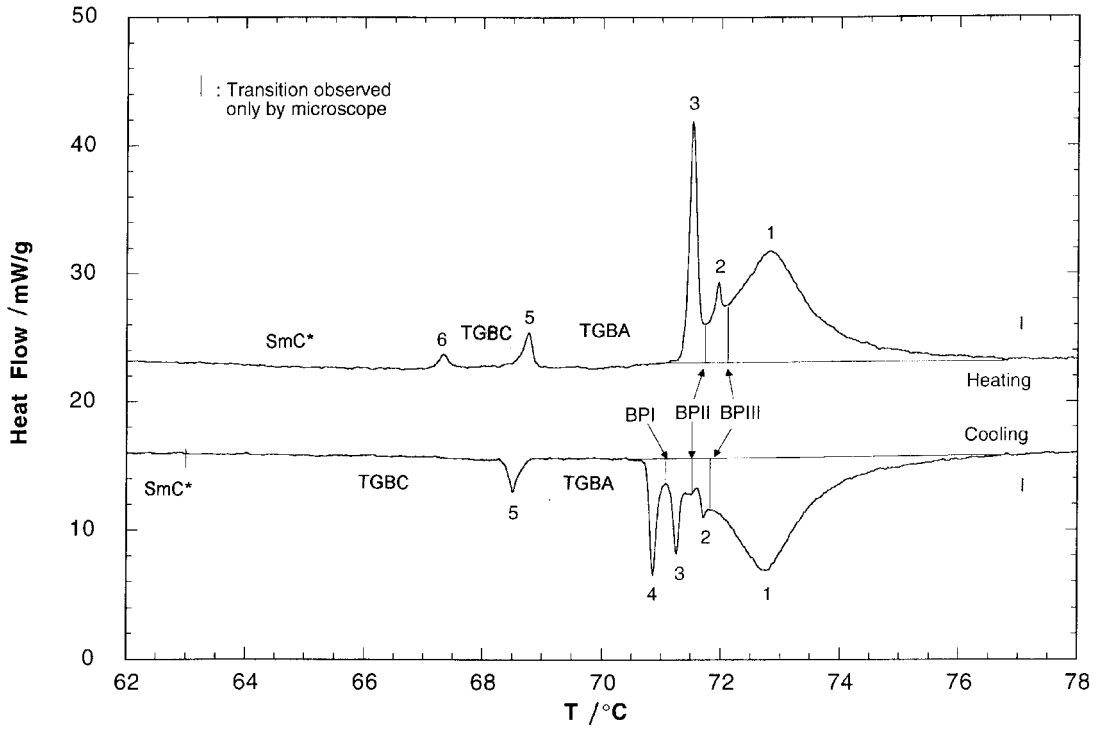

Figure 1. DSC thermograms of (*R*)-FH/FH/HH-18BTMHC on heating and cooling at 0·2°C min^{-1}.

fog texture in the best cases, and is mostly not seen; moreover the platelets of BPI and BPII observed in our compounds already have a grey colour because their helical pitches are very short and the selective reflection is out of the visible range.

For the compounds with a short terminal chain length ($n=13\rightarrow7$), the broad C_p variation 1 and the small peak 2 in the DSC thermograms are always present on cooling (see figure 2 and table 1). They become more and more damped, covering a wider temperature interval which extends from ~6°C ($n=13$) to ~15°C ($n=7$). By analogy with the behaviour of the long chain homologues, we assign the possible blue phases in the compounds $n=13\rightarrow7$ as BPII and BPIII (see table 1). According to this assumption, in the derivatives $n=12\rightarrow7$, only BPIII would exist upon heating. Unfortunately, no blue phases could be observed by microscopy in these short chain homologues and special treatment of the glass plate surfaces did not help. Thus this characterization needs to be verified by further experiments using other appropriate techniques such as selective reflection spectroscopy and the Kossel method.

A further analysis of the DSC data shows that the heat supplied for the broad C_p variation 1 dominates the isotropization process in all members of the series. In the cholesteric blue phases of cholesteryl nonanoate [25, 26, 27] and of *S*,*S*-MBBPC [28], it has already been found that the overall clearing enthalpy of the cholesteric phase through the phase sequence N*–BPI–(BPII–)BPIII–Isotropic is contributed to predominantly by the BPIII–Isotropic transition. To explain this behaviour, it has been proposed that the local order in the blue phases stays close to that of the helical phase N*. The BPIII–Isotropic transition would involve the complete destruction of this local helical nematic order. By making an analogy between our thermodynamic data and the preceding data, we think that the local order of the helical phase previous to the blue phases (interestingly TGBA in our case) could be retained through BPI, BPII and BPIII phases and destroyed only at the BPIII–Isotropic transition. We wonder whether the blue phases exhibit also a smectic-like local order, and discuss this point in the section on X-ray analysis.

Because DSC cannot discriminate pretransitional heat capacity changes and small latent heats, we cannot reach a conclusion on the nature of these blue phase transitions. The sharpness of peaks 3 and 4 suggests first order transitions for BPII–BPI, BPI–TGBA or BPII–TGBA. The more damped transition BPII–BPIII could be a first order transition with a very small latent heat, or a second order transition. Speculation can be made about the nature of the BPIII–Isotropic transition. It could be no transition at all and only a supercritical feature [28]. It could also be second order or perhaps first order [27] for the derivatives with long terminal chain lengths. Studies by high resolution adiabatic calori-

Table 1. Transition temperatures[a] (°C) and enthalpies (in brackets) (KJ mol^{-1}) for (R)-FH/FH/HH-*n*BTMHC (n=20→7) (temperature ratio 0·2°C min^{-1})[b].

n	Mode	Cr		SmC*		TGBC		TGBA		BP I		BP II		BP III		I
20	Heating	•	66·1	—		—		•	69·0 (0·87)	—		•	69·3 (0·28) (3·88)[d]	•	70·0 (2·73)	•
	Cooling	•	55·5	•	[59][c]	•	[64·5][c] (0·051)	•	68·6 (1·04)	—		•	69·1 (0·28) (4·14)[d]	•	70·0 (2·82)	•
18[f]	Heating	•	59·2 (47·9)	•	66·6 (0·048)	•	67·9 (0·108)	•	70·8 (0·69)	—		•	71·4 (0·32) (3·73)[d]	•	72·4 (2·72)	•
	Cooling	•	44·6	•	63[e]	•	67·7 (0·093)	•	70·2 (0·31)	•	70·6 (0·33)	•	71·2 (0·26) (3·70)[d]	•	72·3 (2·81)	•
16	Heating	•	56·3	•	66·6 (0·070)	•	68·0 (0·128)	•	71·5 (0·69)	—		•	72·1 (0·29) (3·43)[d]	•	73·3 (2·45)	•
	Cooling	•	40	•	63[e]	•	67·6 (0·131)	•	70·6 (0·32)	•	71·2 (0·31)	•	71·8 (0·24) (3·42)[d]		73·1 (2·55)	•
14	Heating	•	46·8	•	65·9 (0·051)	•	67·2 (0·043)	•	72·8 (0·57)	—		•	73·6 (0·346) (3·76)[d]	•	74·8 (2·85)	•
	Cooling	•	40	•	61[e]	•	66·9 (0·038)	•	72·1 (0·30)	•	72·3 (0·23)	•	73·2 (0·44) (3·25)[d]	•	74·4 (2·27)	•
13	Heating	•	62	•	64·2 (0·041)	•	64·9 (0·023)	•	71·9 (0·63)	—		•	72·4 (0·23) (2·34)[d]	•	73·9 (1·48)	•
	Cooling	•	30	•	61·5[e]	•	64·6 (0·034)	•	71·3 (0·52)	—		•	72·2 (0·31) (2·40)[d]	•	73·8 (1·57)	•
12	Heating	•	56·5	•	65·2 (0·008)	—		•	74·1 (1·27)	—		—	(2·56)[d]	•	75·7 (1·29)	•
	Cooling	•	25	•	59[e]	—		•	72·6 (0·68)	—		•	73·6 (2·89)[d]	•	74·7 (2·21)	•
11	Heating	•	58	•	66·0 (0·010)	—		•	73·6 (1·11)	—		—	(2·21)[d]	•	75·4 (1·10)	•
	Cooling	•	34	•	60[e]	—		•	71·4 (0·73)	—		•	72·3 (2·60)[d]	•	73·9	•
10	Heating	•	54	•	67·6 (0·014)	—		•	73·2 (0·92)	—		—	(2·05)[d]	•	75·5 (1·13)	•
	Cooling	•	27	•	65·7[e]	—		•	71·7 (0·64)	—		•	72·9 (2·40)[d]		74·6	•
9	Heating	•	58·3	—		—		•	66·7 (0·71)	—		—	(1·94)[d]	•	72·4 (1.23)	•
	Cooling	•	30	•	[53·0][c] (0·041)	—		•	65·1 (0·35)	—		•	67·0 (1·92)[d]	•	71·1	•
8	Heating	•	49·3	•	60·2 (0·010)	—		•	68·0 (0·94)	—		—	(2·06)[d]	•	74·1 (0·83)	•
	Cooling	•	25	•	54·5 (0·050)	—		•	65·7 (0·50)	—		•	68·0 (2·14)[d]	•	73·5	•
7	Heating	•	54·3	—		—		•	60·1 (0·46)	—		—	(1·42)[d]	•	74·3 (0·96)	•
	Cooling	•	25	•	[48·0][c] (0·082)	—		•	56·6 (0·27)	—		•	60 (1·66)[d]	•	67·9	•

[a] Peak temperatures in DSC thermograms were taken as transition temperatures.
[b] Melting and recrystallization temperatures were recorded at 2°C min^{-1}.
[c] Monotropic transition.
[d] Sum of all blue phase transition enthalpies (e.g. n=20, 3·88=0·87+0·28+2·73).
[e] Transition temperatures from microscopic observation only.
[f] One can note that the transition temperatures for n=18 given here are slightly lower than those shown in the figure 1. The reason is that two different samples with slightly different optical purities, prepared from two different batches of (*R*)-2-octanol, were used for the measurements. We have nevertheless kept this discrepancy here because all the other members of the series have been prepared with the same batch of (*R*)-2-octanol.

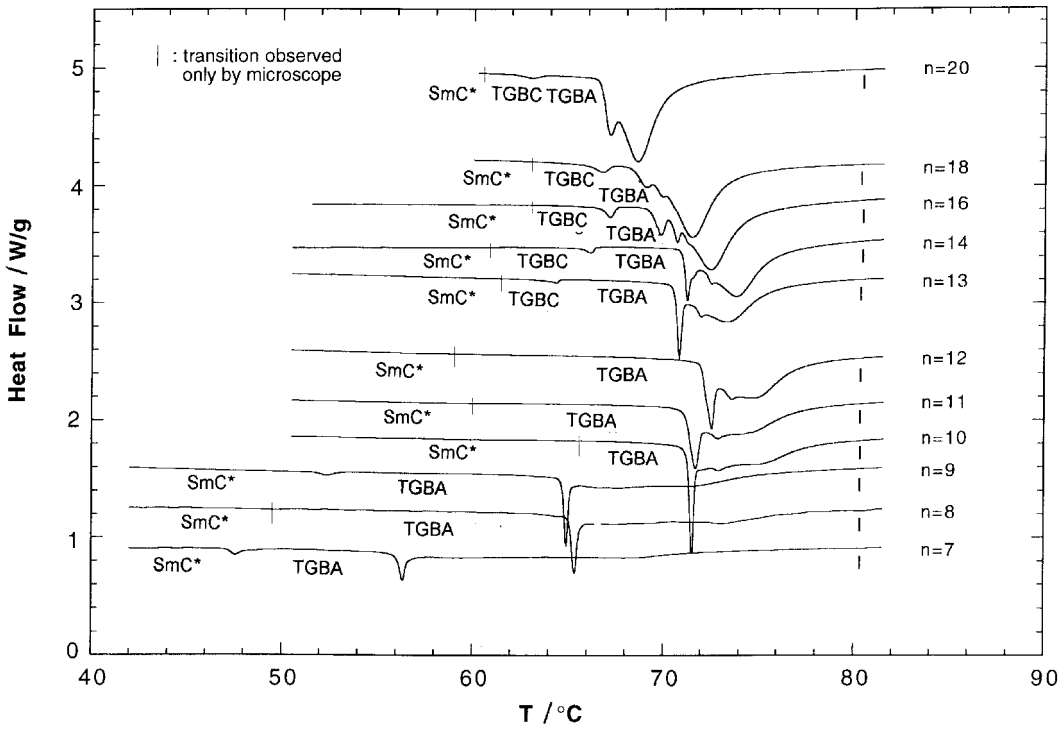

Figure 2. DSC thermograms of all members of the series (*R*)-FH/FH/HH-*n*BTMHC ($n=20\rightarrow7$) on cooling at 2°C min^{-1}.

metry and photopyroelectric techniques are actually in progress on these systems, in order to tackle the above questions.

3.2. *Cr–SmC*–TGBC–TGBA phases*

The TGBA phase is observed in all the members of the series ($n=20\rightarrow7$), whereas the TGBC phase is identified only in the derivatives $n=20$, 18, 16, 14 and 13.

The assignment of the TGBA phase was made by several pieces of experimental evidence: (1) it has characteristic vermis and Grandjean textures; (2) a contact preparation between (*R*) and (*S*) enantiomers shows a SmA texture in the middle [18] (this is confirmed by the SmA phase of the racemic system); (3) helical pitch measurements prove the existence of the helical structure (see §4); (4) X-ray analysis gives evidence of a lamellar structure (see §5).

The TGBC phase has, *a priori*, the same texture as the TGBA phase. Consequently it is difficult to locate the TGBA–TGBC transition by microscopical observation of a sample with no preferred orientation, as usually prepared. Nevertheless, the DSC thermogram shows clearly the TGBA–TGBC transition† (see figure 1) as a small peak on cooling as well as on heating ($\Delta H=0{\cdot}1$ KJ mol^{-1} for the homologue $n=18$). The SmC*–TGBC transition appears in the DSC thermogram performed on heating, but has no signature on cooling. The TGBC phase was definitively identified by helical pitch measurements using well oriented samples (§4): the thermodynamically stable TGBC phase actually exists in a narrow temperature range (≤1°C) located between two small peaks of the DSC thermogram (between peaks 5 and 6 in figure 1); upon cooling, the TGBC phase persists over a larger temperature domain of several degrees (up to 6°C) in a metastable state. X-ray diffraction studies (§5) confirm this assignment of TGBC by optical observations.

The transition TGBC–SmC* is clearly observed by microscopy with the appearance of the pseudo-homeotropic and broken fan-shaped textures. The SmC* phase occurs in almost all members of the series, preceding the TGBC phase in the cases of $n=18$, 16, 14, 13 and preceding the TGBA phase in the other cases. There are three exceptions ($n=20$, 9, 7) where the transition Cr–TGBA takes place directly on heating. However the SmC* phase is formed upon cooling.

3.3. *Phase diagrams for enantiomers and racemic mixtures*

We summarize discussion on the mesomorphic properties of the series in a phase diagram as a function of terminal chain length *n* (figure 3). Firstly, it is interesting to note the 'up then down' evolution of the various transition temperatures for the overall clearing process

† We rectify slightly here results for the TGBC–SmC* transition given in a previous communication [18].

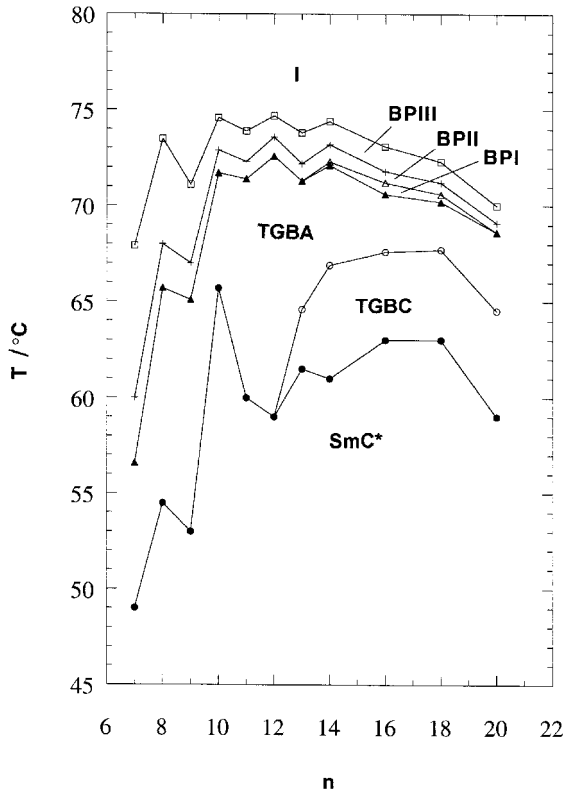

Figure 3. Phase diagram of the series (*R*)-FH/FH/HH-*n*BTMHC as a function of terminal chain length *n*. The continuous lines are simply guides for the eye.

(from TGBA to I): when $n \leqslant 12$, the clearing temperatures increase with increasing *n* and an odd–even effect is visible; they then decrease when *n* increases from 12 to 20. This phenomenon was not reported for other TGB series [29, 30]. We have no explanation for this difference.

We depict the phase behaviours of the racemic mixtures (table 2) as a function of the chain length *n* in figure 4. Only four homologues were prepared, but the same evolution of the clearing temperatures with *n* was observed as in the phase diagram for the enantiomers. The special feature of this racemic diagram is the appearance of the nematic phase (N) when $n \leqslant 14$, which was not expected considering that no cholesteric phase (N*) exists for the corresponding enantiomers. Therefore to consider the phase behaviour as a function of chirality would be more complicated when $n \leqslant 14$.

4. Helical pitch measurements

Pitch measurements have been performed microscopically for all the compounds of the series. The same phase sequences have been observed as in the DSC study.

In the TGB phases the measurements were carried out using the Grandjean–Cano method, with a prismatic cell, in the planar orientation [31, 32]. The planar orientation had to be kept all through the measurements, but generally when cooling from blue phases to the TGBA phase, the liquid crystal changed partly into pseudo-homeotropic orientation in the TGB phases. We had consequently to avoid any transition from the TGBA phase to blue phases. The sample had to be prepared in the TGB temperature range, and cooled just after its preparation. Measurements were thus performed first on cooling from the middle of the TGBA range down to the TGBC–SmC* transition. They were afterwards performed on heating across the whole range of the TGBC and TGBA phases. It was observed that the pitch values measured on cooling and on heating at the same temperature in the same phase are very close to each other (see figure 5 (*a*), 5 (*b*) and 5 (*c*)).

We can readily discriminate the TGBC phase from the TGBA phase in optical observations of the sample in the planar orientation in a prismatic cell. The TGBA–TGBC transition is marked by a sudden change of pitch (a sharp increase on cooling), approaching a discontinuity. If the temperature varies very slowly, it is however possible to show that this transition is really continuous; figure 6 shows this clearly. In this way we identified TGBC phases in the homologues with $n=20$, 18, 16, 14 and 13.

In a similar way to that observed by DSC and microscopy, the SmC*–TGB transition occurs at a higher temperature on heating than on cooling; the shift can reach 5 degrees. In other words TGBC phases exist over a larger temperature range upon cooling than upon heating.

In the SmC* phase, the pitch measurements are also performed using the Grandjean–Cano method in a prismatic cell, when this is allowed by the pitch range ($p > 0{\cdot}13\,\mu m$). In this case the liquid crystal must be in the pseudo-homeotropic orientation [33]. If $p < 0{\cdot}13\,\mu m$, neither selective reflection colours nor Grandjean–Cano steps are visible. The pitch measurements are then performed on a free surface drop [33], observing the Friedel fringes as for a SmC* phase [34]. In both cases measurements are carried out on heating.

In a prismatic cell, the SmC*–TGB transition temperature is much higher in the pseudo-homeotropic orientation than in the planar orientation. For a drop, in the pseudo-homeotropic orientation this temperature is also higher; this is due on the one hand to the different orientations, and on the other hand to the small thickness of the drop. Measurements are indeed performed on very thin regions, where surface effects unwind TGB phases. In the pseudo-homeotropic orientation and in a confined geometry, a SmC* domain encroaches the TGB domain. These points explain the difference between the

Table 2. Transition temperatures[a] (°C) and enthalpies (in brackets) (KJ mol^{-1}) of racemic FH/FH/HH-*n*BTMHC ($n=18$, 14 and 9) (temperature rate 0·2°C min^{-1}).

n	Mode	Cr		SmC		SmA		N		I
18	Heating	•	68·1 (59·3)	•	70·7 (0·045)	•	74·0 (4·34)	—		•
	Cooling	•	49·5 (53·6)	•	70·3 (0·084)	•	73·4 (4·26)	—		•
14	Heating	•		•	68·8 (0·048)	•	75·2[b]	• (3·21)[c]	75·4	•
	Cooling	•		•	68·8 (0·049)	•	75·1[b]	• (3·23)[c]	75·3	•
9	Heating	•		•	53·3 (0·063)	•	69·1 (1·16)	• (2·16)[c]	74·5 (1·00)	•
	Cooling	•		•	53·1 (0·02)	•	68·8 (1·06)	• (2·02)[c]	74·2 (0·95)	•

[a] See note [a] in table 1.
[b] The very narrow temperature range of the N phase ($\Delta T \approx 0{\cdot}2$°C) is obtained from microscopic measurement, but could not be discriminated by DSC.
[c] Sum of the transitions SmA–N–I.

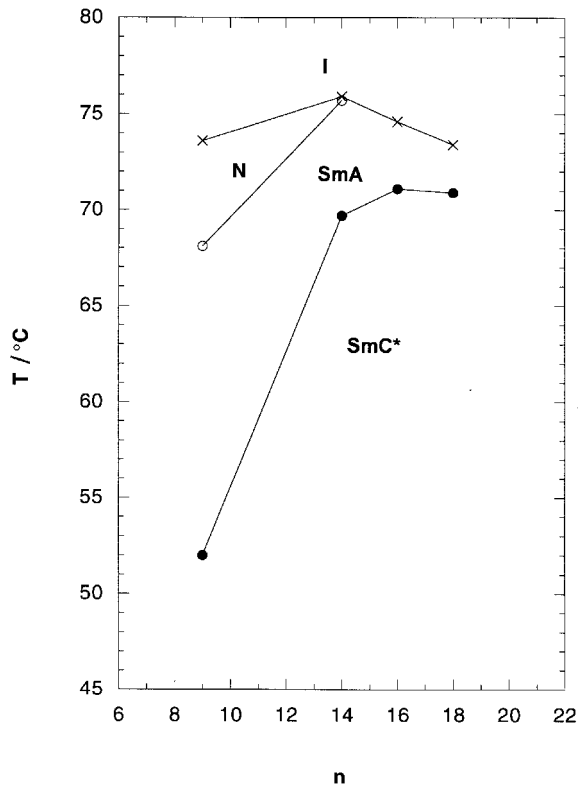

Figure 4. Phase diagram of the racemic mixtures of FH/FH/HH-*n*BTMH as a function of terminal chain length *n*. The continuous lines are simply guides for the eye.

transition temperatures observed in the two types of measurement.

For all the phases studied, colours are visible, produced by selective reflection of visible light. In the TGBC and TGBA phases visible wavelengths with $\lambda = np$ are reflected when the pitch is between 0·5 μm (red) and 0·25 μm (violet). In the SmC* phase visible wavelengths with $\lambda = np$ are again reflected when the pitch is between 0·5 μm (red) and 0·25 μm (violet), and also with $\lambda = 2np$ when the pitch is between 0·25 μm (red) and 0·13 μm (violet).

We now give the results of the helical pitch measurements for homologues $n=18$, 13 and 9.

4.1. *Pitch values for n=18*

The compound with $n=18$ exhibits all the phases observed for the series. Figure 5(*a*) shows the pitch evolution versus temperature in the different phases. On heating in a prismatic cell the SmC* phase ranges from about 45 to 64·7°C in the planar orientation, and to 67·1°C in the pseudo-homeotropic orientation. Its pitch is big enough to produce selective reflected visible light. The Grandjean–Cano method can thus be used in this case. The pitch is almost constant, with a value of 0·27 μm from 48 to 65°C; it decreases between 66 and 67·1°C, reaching 0·24 μm. The liquid crystal phase is violet ($\lambda = np$) at low temperature, and becomes dark red, and red ($\lambda = 2np$) near the transition to the TGBC phase.

Upon heating, the TGBC phase with a pitch value of

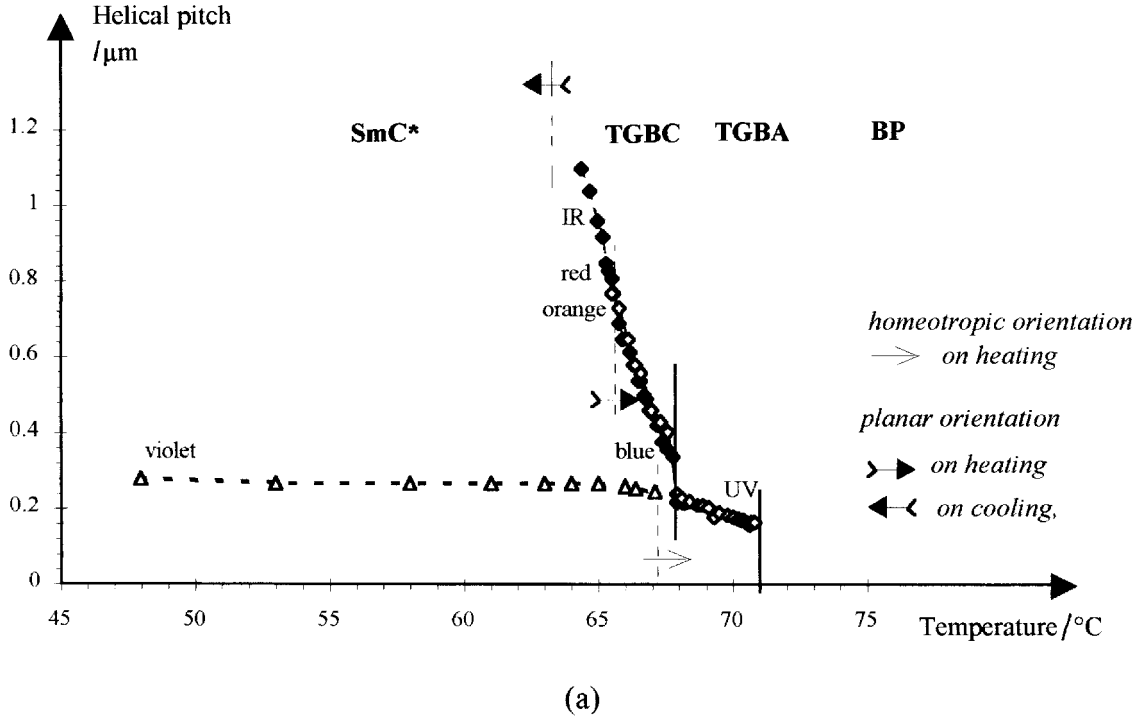

Figure 5. (*a*) $n=18$, (*b*) $n=13$, (*c*) $n=9$: helical pitch versus temperature, in the TGBA, TGBC and SmC* phases. In TGB phases measurements were performed using a prismatic cell in the planar orientation: on cooling (◆) and on heating (◇). In the SmC* phase measurements were both carried out on the pseudo-homeotropic orientation on heating: in a prismatic cell (△) and on a free surface drop (●). Selective reflection colours are displayed in the figures. The TGBC–SmC* or TGBA–SmC* transition occurs at higher temperature on heating than on cooling in the prismatic cell with planar alignment. Moreover, these transitions are observed at different temperatures when measurement is done on the homeotropic orientation. (Transitions are marked by dotted lines with arrows.) The TGBA–TGBC transition is revealed by a sudden pitch increase on cooling; no shift occurs between measurements on cooling and on heating in this case (a solid upright line indicates the transition).

0·76 μm is formed near the SmC*–TGBC transition at 65·5°C. Then the pitch decreases with increasing temperature in the TGBC phase to 0·32 μm at 67·9°C. The sample in the TGBC phase is colourless at low temperature, and becomes blue ($\lambda=np$) near the TGBA transition. Upon cooling, the TGBC phase persists below 65·5°C. The pitch value continues to increase with decreasing temperature; it seems to diverge at the approach of the TGBC–SmC* transition (63·3°C). Measurement becomes very imprecise when the pitch value becomes larger than 1 or 1·5 μm, and we do not give data in the figure.

The TGBA phase ranges from 67·9 to 70·8°C. Its pitch decreases with increasing temperature, but less quickly than in the TGBC phase. The pitch value is about 0·24 μm at 68·1°C and diminishes to 0·16 μm at 70·8°C. The liquid crystal phase is violet at low temperature and colourless from 68·1 to 70·8°C ($\lambda=np$).

4.2. *Pitch values for n=13*

The compound with $n=13$ displays all the phases observed in the series, except for one of the blue phases. Figure 5(*b*) shows the pitch evolution in the different phases as a function of temperature.

Upon heating, the SmC* phase ranges from about 30 to 64·3°C in a prismatic cell in the planar orientation and to 65·6°C in a drop. Its helical pitch has values smaller than that for $n=18$; they are less than 0·13 μm. For this reason pitch measurements have been made using both methods: for a drop close to the transitions, and in a prismatic cell in the middle of the temperature domain. The pitch is about 0·07 μm at 31·6°C and increases up to a plateau: its value is 0·13 μm from 44·6 to 56·6°C. It then decreases to 0·07 μm at 64·1°C. The liquid crystal phase is colourless at low temperature, becomes black with violet Grandjean–Cano threads on the plateau ($\lambda=2np$), and is again colourless at high temperature; this corroborates the pitch values.

The TGBC phase of the compound with $n=13$ has the same behaviour as for $n=18$: upon heating, the SmC*–TGBC transition occurs at 64·3°C with a rather short pitch of 0·6 μm; afterwards, the pitch decreases to 0·48 μm at 65·6°C near the TGBA phase. Upon cooling, the pitch increases with decreasing temperature: it reaches

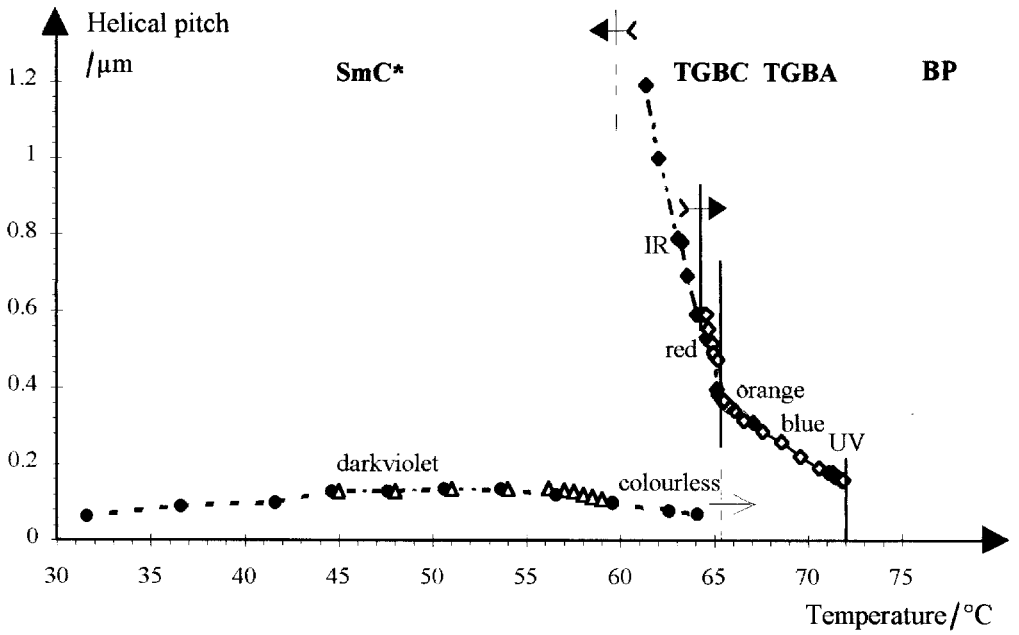

(b)

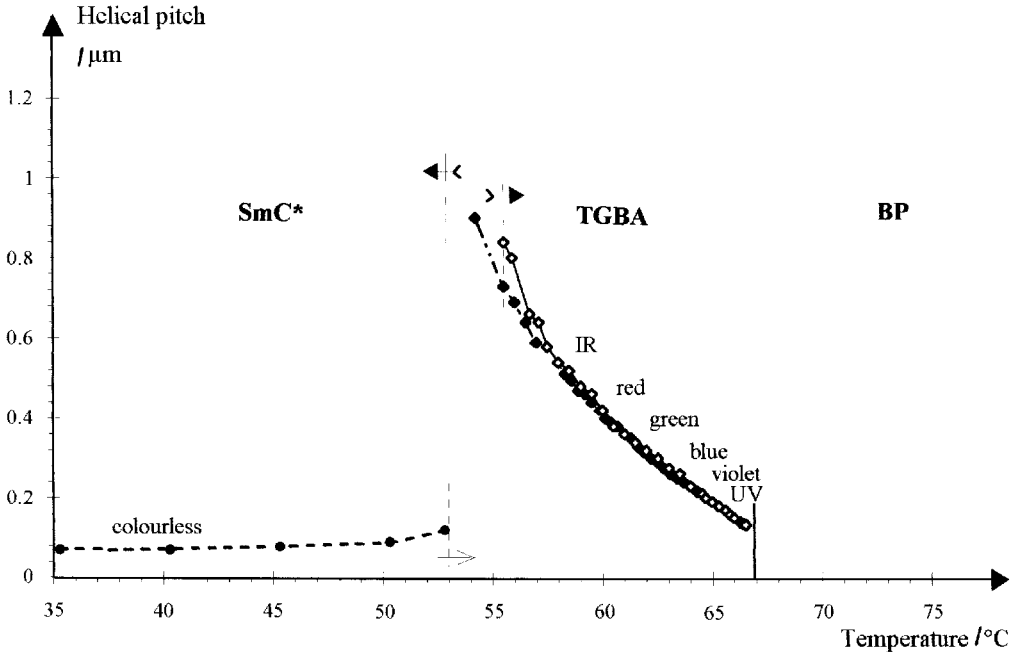

(c)

Figure 5. (*continued*).

1·19 μm at 61·4°C and diverges at the TGBC–SmC* transition (≈60°C). The liquid crystal phase is colourless at low temperature and exhibits red coloured selective reflection ($\lambda = np$) at high temperatures.

The TGBA phase occurs from 65·6 to 71·9°C. Its pitch decreases from 0·37 μm at 65·6°C to 0·16 μm at the transition to the blue phases. The liquid crystal phase exhibits selective reflection colours from orange to UV ($\lambda = np$). The small pitch values at high temperature make it colourless over about 3·3°C.

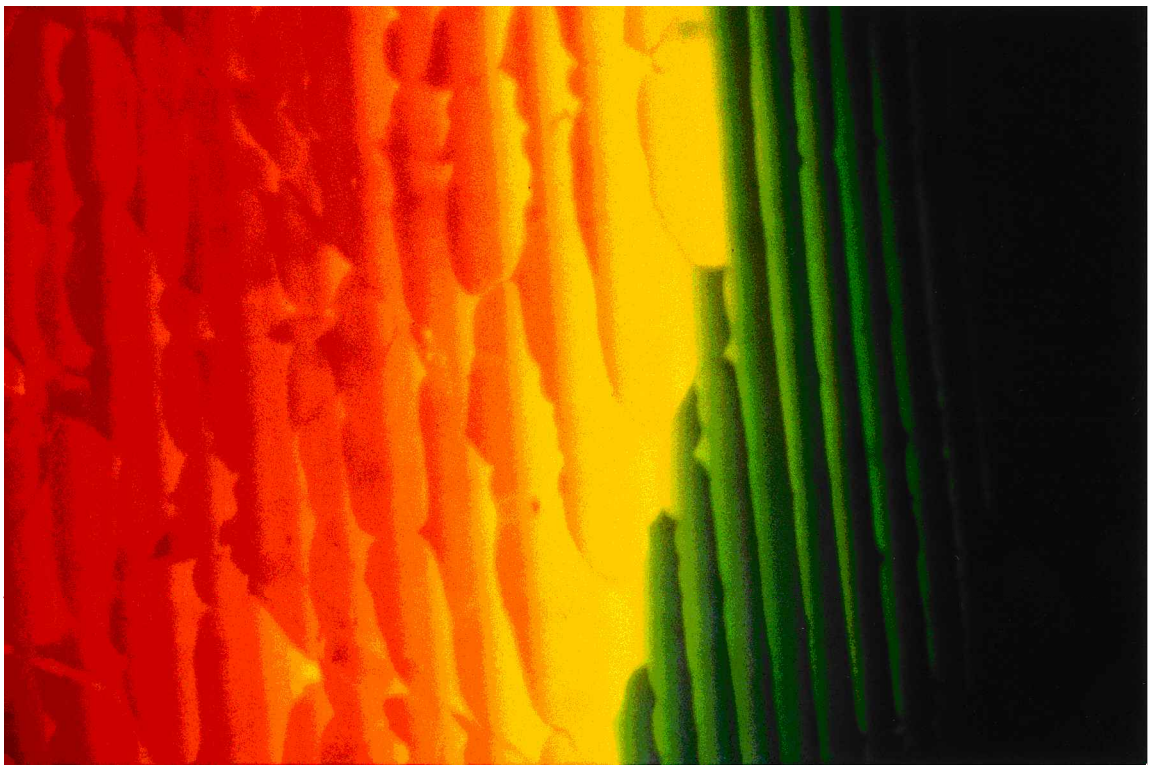

Figure 6. Grandjean–Cano lines in a prismatic cell at the TGBA–TGBC transition for the compound with $n=14$. The part exhibiting a green colour ($P\approx0{\cdot}30\,\mu m$) is in the TGBA phase and the part exhibiting an orange colour ($P\approx0{\cdot}54\,\mu m$) in the TGBC phase. Here the temperature was changed so slowly that the narrow spaced green lines of TGBA transferred continuously to the large spaced orange lines of TGBC.

4.3. *Pitch values for n=9*

The compound with $n=9$ exhibits only some of the phases observed for the series. The TGBC phase and one of the blue phases do not appear in the sequence. Figure 5 (*c*) shows the pitch evolution versus temperature in the different phases.

The SmC* phase ranges from 30 to 55·2°C. Its pitch is much smaller than for the other compounds, always less than 0·13 μm; only the measurements on a drop can be used to evaluate it. It increases from 0·07 μm at 35·3°C to 0·12 μm at 52·8°C. The sample exhibits no selective reflection colour.

The TGBA phase occurs from 55·2 to 66·7°C on heating, and from 66·5 to 53°C on cooling. Its pitch decreases with increasing temperature, from 0·9 μm at 54·2°C to 0·13 μm at 66·5°C. The liquid crystal phase is colourless (IR) at low temperature, sweeps the visible reflection spectrum ($\lambda=np$) from red to violet, and is again colourless (UV) over 2·5°C, from 64 to 66·5°C, where the pitch varies from 0·23 to 0·13 μm.

4.4. *Discussion*

Helical pitch measurements in the TGBC phase clearly show that the SmC*–TGBC and TGBC–SmC* transitions are different: the TGBC structure suddenly winds up on heating, whereas it gently unwinds at lower temperature on cooling. This probably explains why the enthalpy associated with the SmC*–TGBC transition is bigger than that associated with the TGBC–SmC* change (the latter is too small to be measured in our DSC experiment). As regards the values of the pitches, we note that the helical pitches in the different phases exhibited by all the members of this series are generally very small.

In the SmC* phase for $n=7$ to 12, the liquid crystal phase displays no selective reflection colours. The pitch remains lower than 0·12 μm, and reaches 0·06 μm. To our knowledge the smallest SmC* pitch observed up to now in comparable series was about 0·15 μm, after a fall just below the SmC*–TGBA transition [35].

In the TGBC phase close to the transition to the TGBA phase, the helical pitch value lies between 0·48 μm (for $n=13$) and 0·22 μm (for $n=20$). The smallest pitch observed in comparable series was about 0·4 μm [36].

In the TGBA phase the pitch values at the TGBA–BP transition are between 0·14 and 0·2 μm. The smallest pitch previously observed in a TGBA phase was about 0·4 μm [32] and 0·38 μm [4], although in a different

type of series—a chiral, non-polar symmetric dimesogen—the TGBA phase exhibits a smaller pitch of 0·24 μm [37].

We think that the very small helical pitch in the TGBA phase is the reason for the direct transition from the TGBA phase to the blue phases. In this case of very high chirality, the double twist structure of the blue phase should be more stable than the simple twisted structure of the N* phase.

5. X-ray structural analyses

5.1. *On a powder sample*

A powder sample was prepared in a 1 mm diameter Lindemann capillary using the $n=9$ homologue. X-ray scattering experiments were performed using CuK_α radiation from an 18 KW rotating anode X-ray generator (Rigaku RU-200); a flat germanium (1 1 1) monochromator was used. The incident beam was a $0{\cdot}6 \times 0{\cdot}6\,mm^2$ spot on the sample and the diffracted beam was detected by a two-dimensional image plate system. The instrumental resolution was about $1{\cdot}0 \times 10^{-2}$ Å^{-1} FWHM (full width at half maximum) along the horizontal as well as the vertical direction. The sample temperatures were controlled within a 0·1 K accuracy.

The variation with temperature of the layer spacing d ($d=2\pi/Q_0$) and of the FWHM of the Bragg peaks was recorded upon cooling for the $n=9$ homologue (see figures 7 (*a*) and 7 (*b*)). In the biphasic domain of isotropic and blue phases, diffuse scattering reveals the existence of short range smectic order. From isotropic phase to blue phases, the layer spacing increases continuously from 35·6 Å ($T=75$°C) to 38·7 Å ($T=69$°C), while the FWHM of the diffraction peak decreases from $1{\cdot}0 \times 10^{-1}$ to $1{\cdot}4 \times 10^{-2}$ Å^{-1} and the intensity of the peak increases sharply (by six times). Then the value of d remains stable (38·9 Å) in the blue phases covering a temperature range of about 4°C. At the BP–TGBA transition, the layer distance changes from 38·9 Å to 39·2 Å within a 1·8°C interval, and then it decreases slightly to 39·0 Å in the TGBA phase within 10°C. There is a sudden drop of the value of d (from 39·0 to 38·1 Å within 2°C) at the TGBA–SmC* transition. In the SmC* phase, the layer distance continues to decrease upon cooling and the Bragg peaks becomes resolution limited.

Even in the TGBA phase, the layer distance is still remarkably lower than the total extended molecular length (45·3 Å); this underlines that there is not an all-*trans*-conformation of the alkyl chains in the molecule. Using the value of d in the TGBA phase, we calculated the tilt angle in the SmC* phase and obtained an apparent tilt angle of 13·3° at $T=53$°C and of 14·8 at $T=50$°C.

What is new here is the existence of some layer structure in the blue phases. Figure 7 (*b*) shows clearly

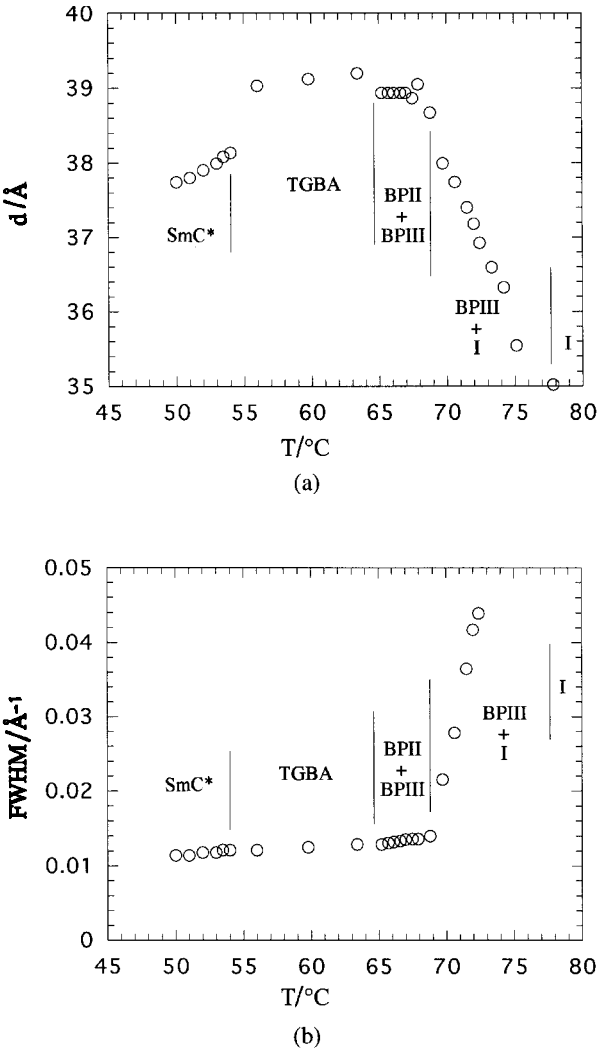

Figure 7. (*a*) Layer spacing d of the smectic order versus temperature; (*b*) FWHM of the Bragg peak versus temperature for (*R*)-FH/FH/HH-9BTMHC.

that the characteristic width of the diffraction peak in the BPII and BPIII phases is of the same order as that in the TGBA phase. A simple evaluation of the correlation length from $\xi=2/\text{FWHM}$ is not very accurate here, because the width is not much larger than the instrumental resolution (about $1{\cdot}0 \times 10^{-2}$ Å^{-1}). Nevertheless, we can conclude that the average correlation length of the smectic order in the blue phases is qualitatively comparable with that in the TGBA phase, and much bigger than that in the mixture of isotropic and BPIII phases.

High flux X-ray experiments have been carried out to study in detail the smectic-like order in the blue phases of this series. Figure 8 shows the layer spacing and the FWHM of the Bragg peak in the blue phases of the

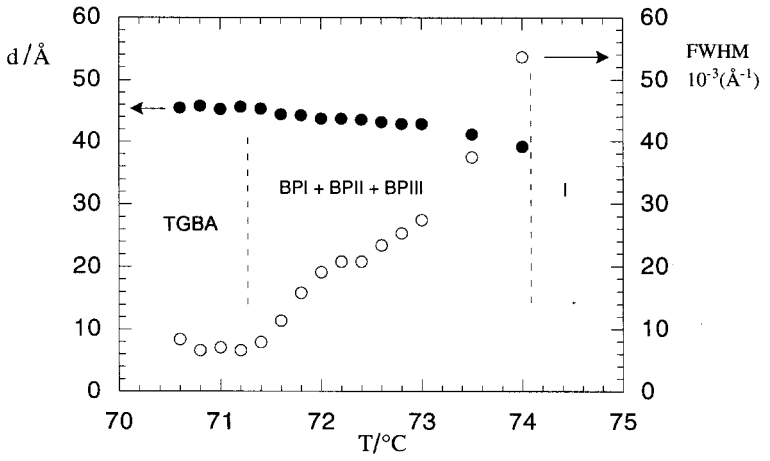

Figure 8. Layer spacing d of the smectic order (●) and FWHM of the Bragg peak (○) in the blue phases of (*R*)-FH/FH/HH-18BTMHC. The position of the transition BP–TGBA (marked by a dotted line) is approximate (see ref. [38]).

homologue $n=18$. The detailed discussion is published elsewhere [38].

5.2. *On an oriented sample*

For the homologue $n=13$, the helical pitch in the TGBC phase is much bigger than that in the SmC* phase (about ten times). Therefore, the size of the smectic blocks (l_b) in TGBC may be of the order of the SmC* pitch. If the helical structure of the smectic C* phase occurs under the same conditions as in a SSFLC cell [39], this compound may exhibit a TGBC* phase, with a SmC* twist occurring within the smectic blocks. Although predicted by the RL model, such a phase has been detected neither by DSC studies, nor by optical observation. X-ray scattering could give more structural information and allow us to obtain evidence of an unusual TGBC structure that could be TGBC*.

The X-ray measurements were therefore made on a well aligned sample of $n=13$. The cell was formed of two glass plates coated with PVA and gently buffed unidirectionally; it was filled with the sample in the isotropic state by capillarity. Its thickness was determined by two parallel gold wires of $\varnothing$ 25 μm. The planar orientation was checked by optical observation. The cell was then mounted in a two-stage oven which provided temperature control within a 10 mK accuracy.

The same source of X-rays as in the experiment on the powder sample was used, and the sample was mounted on a four-circle goniometer. A flat pyrolytic graphite monochromator was used; the scattered intensity was analysed by vertical slits and collected by a scintillator. The resolution was set to $1{\cdot}7\times10^{-2}$ Å^{-1} in the longitudinal plane. The angular vertical resolution $\Delta\chi$ defined by a series of slits was set to 14·8° (FWHM) with a 1×2 mm^2 beam for ω scans. It was improved to 7·4° (FWHM) with a 1×1 mm^2 beam for χ scans (see the inset of figure 9 for a definition of the ω and χ rocking angles).

The sample was first cooled from isotropic to the TGBA phase and then studied on cooling through the TGBA and TGBC phases. The scattering vector **Q** determined from longitudinal Q_z scans was about $Q_0=0{\cdot}156\pm0{\cdot}017$ Å^{-1}. Note that a broad longitudinal resolution ($1{\cdot}7\times10^{-2}$ Å^{-1}) was chosen to avoid a small 2-*theta* correction with temperature within the TGB domain.

5.2.1. *ω Scans*

A series of texture scans (ω scans) was performed on cooling from about 71 to 61°C throughout the TGBA, TGBC, and SmC* phases. Figure 9 shows a typical ω scan in the TGB phases through the Bragg maximum at $Q_z=Q_0$. In the TGBA phase at 67·4°C, the diffraction peak is centred along the direction perpendicular to the pitch axis ($\omega=0$) and well fitted to a Gaussian function of characteristic width $\sigma_G=12{\cdot}7°$, which is well above the instrumental resolution $\Delta\omega$ (better than 1°).

In the TGBC phase ($T=64{\cdot}4$°C in figure 9), the signal splits up into two separate peaks at position $\omega_L=\pm13{\cdot}1°$. This behaviour is similar to that of previous observations on other TGBC phases [9] and corresponds to a tilt of the layers relative to the pitch axis direction. The signal is better fitted to Lorentzian profiles of characteristic half width $\sigma_L=4{\cdot}7°$. The tilt angle ω_L is plotted against temperature in figure 10. In the TGBA phase the peaks are centred around $\omega=0$ indicating that the smectic layers are parallel to the helical axis. A sudden increase characterizes the TGBA–TGBC transition. Within the TGBC domain, the tilt increases from 10° at 65·3°C to 15° at 63·1°C.

The evolution of the half width at half maximum (HWHM $=(\ln 2)^{\frac{1}{2}}\sigma_G$ for TGBA, and HWHM $=\sigma_L$ for TGBC) is plotted versus temperature on figure 11. The trend is a decrease with temperature. The width falls off gently within the two TGB phases and exhibits an abrupt jump across the TGBA–TGBC transition.

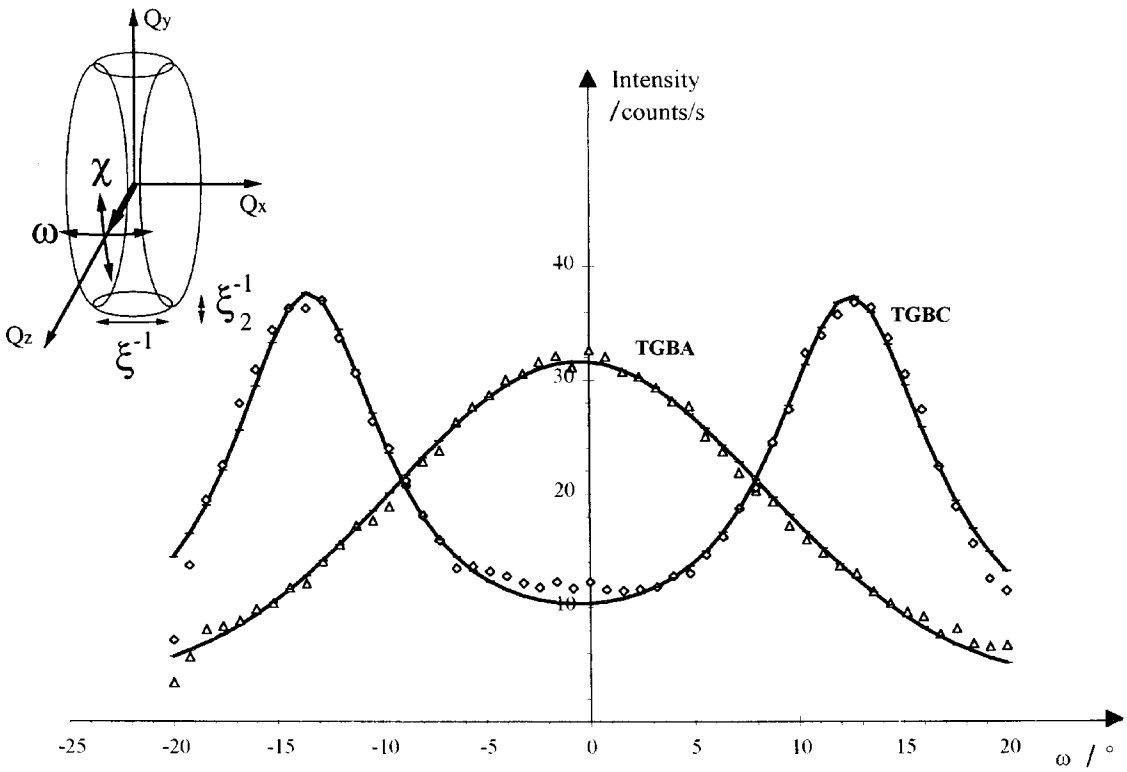

Figure 9. ω scans for the TGBA and TGBC phases, through the Bragg maximum at $Q_z = Q_0$: X-ray scattered intensity versus ω; inset shows the scattering directions. Q_x corresponds to the helical axis; ω and χ scans are rotations about the Q_y and Q_x axes, respectively. (△): $T = 67{\cdot}4$°C in the TGBA phase, about 2°C above the TGBA–TGBC transition. The solid line is a fit to a Gaussian profile, centred at $\omega = 0$ and of characteristic halfwidth $(\ln 2)^{\frac{1}{2}}\sigma_G = 10{\cdot}6°$. (◇): $T = 64{\cdot}5$°C in the TGBC phase, about 1° below the TGBA–TGBC transition. The solid line is a fit to two symmetrical Lorentzian profiles, centred at $\omega \approx \pm 13°$ and of characteristic halfwidth $\sigma_L = 4{\cdot}7°$.

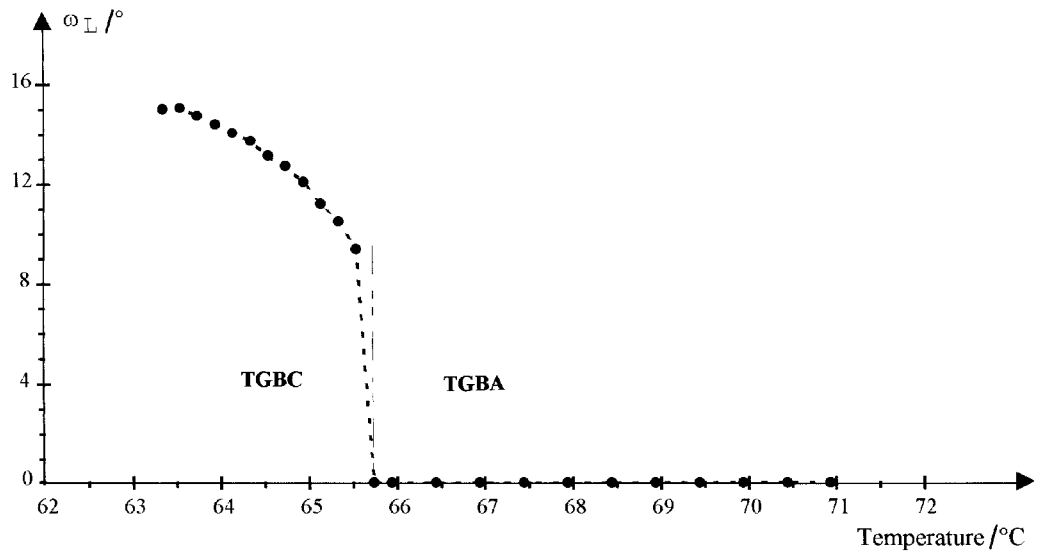

Figure 10. Tilt angle ω_L relative to the screw axis versus temperature, in the TGBA and TGBC phases. ω_L corresponds to the angular position of the diffraction peak in ω scans. A single centred peak occurs in the TGBA phase; it splits into two symmetrical peaks in the TGBC phase.

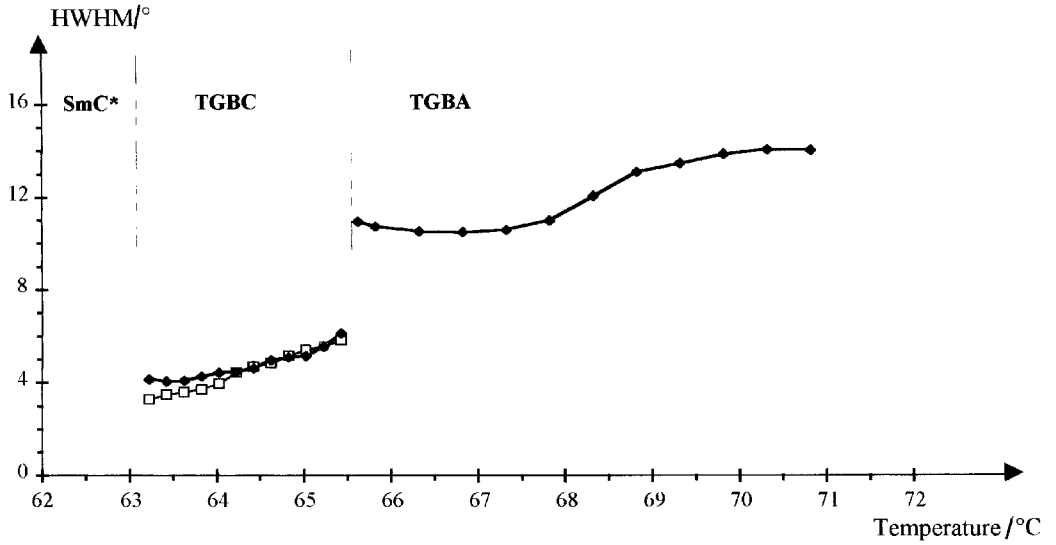

Figure 11. Characteristic HWHM versus temperature in the TGBA, $(\ln 2)^{\frac{1}{2}}\sigma_G$, and TGBC ($\sigma_L$) phases in ω scans. σ_G and σ_L are obtained from the fit of the data obtained at different temperatures. In the TGBC phase, the HWHM of both the left and right wings are given with two different symbols.

Furthermore we notice that the decay of the width is not uniform throughout the TGBA phase, but changes from 14° to 10° around 68·5°C. The discontinuous jump occurring at the TGBA–TGBC transition may suggest that this transition is first order; however a sharp but continuous evolution cannot be ruled out since our steps in temperature (0·2°C) are certainly too large close to the transition.

5.2.2. *χ Scans*

A series of χ scans was then performed on cooling in the TGBC domain. Figure 12 shows a χ scan recorded at 63·3°C. It exhibits a series of regularly spaced maxima characteristic of a commensurate TGB structure. The angular difference between two smectic blocks is about 16·4°, consistent with 22 blocks per pitch in the TGBC structure. This value remains constant over all the TGBC domain, whereas for a previously studied series [8], the number of blocks in a pitch increases from 16 to 18 and 20 with decreasing temperature. Furthermore all the spectra obtained can be superposed with good agreement: no angular shift has been observed with decreasing temperature.

The contrast of the modulation (I_{MAX}/I_{MIN}) found about 1·55 is worth comment. Its value depends on (1) the natural width of the Bragg reflection along χ, (2) the experimental resolution in χ and (3) the mosaicity of the sample. The natural width along χ, controlled by Landau–Peierls fluctuations [40], is well below our experimental resolution. The contribution of the resolution can be estimated by a simulation of a χ scan as a series of Dirac functions (equispaced Bragg spots) convoluted by the resolution function along the χ coordinate (Lorentzian shape of width 7·4° FWHM). The contrast would then be about 2·7, i.e., significantly larger than the measured values; we therefore conclude that the mosaicity plays a role. Whether the mosaicity is an angular spread of the reflections from commensurate regions or a mixture of commensurate and incommensurate zones is not distinguishable [41].

5.2.3. *Discussion*

By combining the number of the smectic blocks and the pitch values given in § 4, we can calculate the block width ($l_b = p(T)/22$) in the TGBC phase. The block width grows with decreasing temperature (see figure 13): l_b increases regularly on cooling, from 200 Å at 65°C to 500–600 Å at 61·4°C. The width σ of the intensity profile in the ω scans (figure 11) results from the broadening (of the order $\pi/Q_0 l_b$) of the Bragg reflection due to the finite size l_b of the smectic slabs; this σ value may be increased by the angular spread of the helical axis x. The estimated width ($\pi/Q_0 l_b \approx 6°$) is consistent with the experimental value at $T = 65{\cdot}5$°C, but lower than the value at $T = 63{\cdot}3$°C (2° instead of 4°). We can evaluate the angular distribution of the helical axis in the sample as of the order of 2° at most.

In the TGBA phase, l_b cannot be measured since the TGBA structure is not commensurate. Taking $l_b = l_d$ (l_d being the distance between two consecutive screw dislocation lines), we can estimate that $l_b = (dp/2\pi)^{\frac{1}{2}} = (p/Q_0)^{\frac{1}{2}}$ [1]. We have in this case $l_b = 100$–150 Å. This then gives an estimated broadening ($\pi/Q_0 l_b$) lying between 11·4° near the transition to the blue phases and

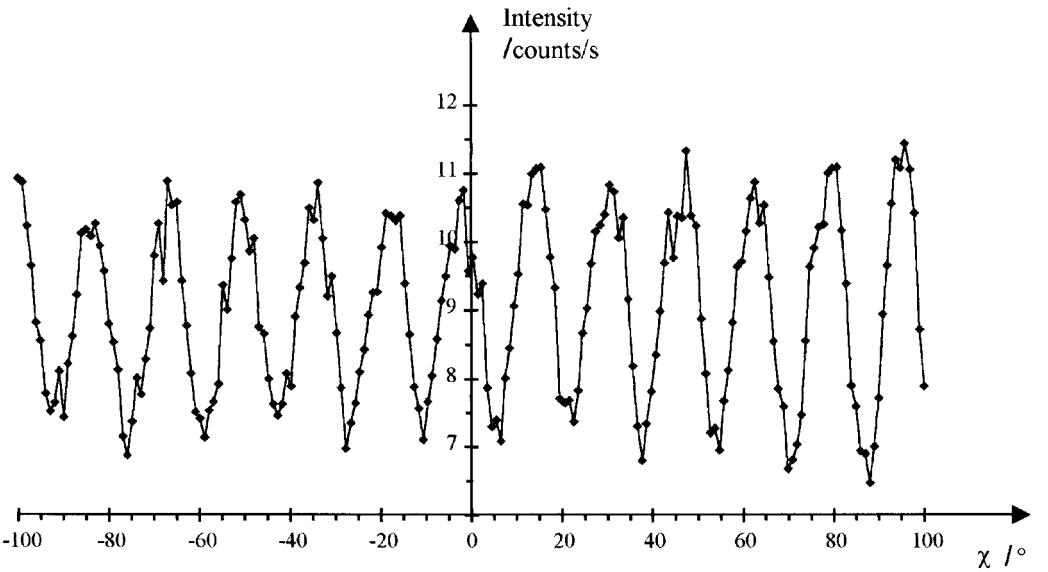

Figure 12. χ scans in the TGBC phases: X-ray scattered intensity around the diffraction ring. The scan displayed was done at $T=63{\cdot}3°C$; similar data were obtained over the entire temperature domain of TGBC. The angular difference between two consecutive peaks is about 16·4° and that is consistent with 22 blocks per pitch.

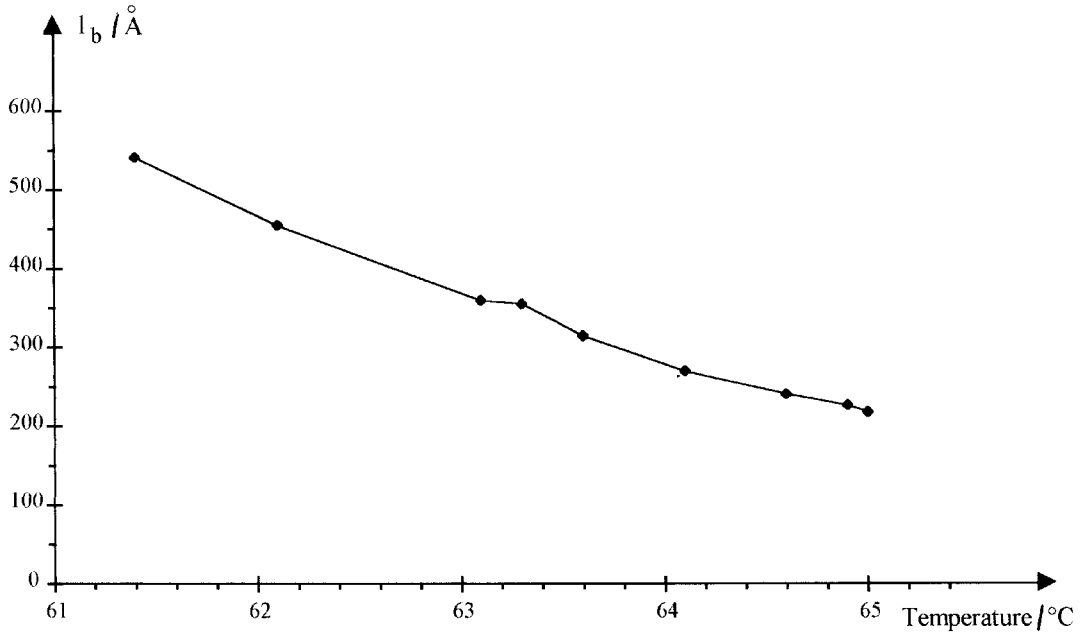

Figure 13. Blocks width (l_b) versus temperature. l_b is obtained from the pitch measurements in the TGBC phase, with a constant block number of 22 per pitch. l_b increases from 200 Å to about 600 Å with decreasing temperature.

7·5° at the transition to the TGBC phase. The experimental values decrease from 14° at 72°C to 10·7° at the transition to the TGBC phase, that is a little higher. From this estimation, the broadening of the Bragg reflection due to the limited size of the blocks is not sufficient to explain the experimental σ values; other factors (such as the angular distribution of the helical axis and the imperfect alignment of the sample) can induce such a difference. The decrease of the σ value with decreasing temperature may be due to the improvement of the sample alignment and the helical axis distribution upon cooling.

The results of this study are quite similar to those previously obtained for other series [8, 9, 36]. The TGBC and TGBA phases exhibit qualitatively identical ω scans to those of other TGB materials studied. The

smectic layers are parallel to the helical axis in the TGBA phase, and are tilted relative to the helical axis in the TGBC phase. The TGBC phase also displays commensurate χ scans, with 22 blocks per pitch. The only difference lies in the evolution with temperature: χ scans are commensurate over all the temperature domain, the number of blocks per pitch remains constant, and no angular shift is observed.

The compound with $n=13$ was chosen for this study because of its high chirality, and the large difference between the pitch values in the SmC* and TGBC phases. With 22 blocks per pitch, l_b reaches at most 500–600 Å. This value is still a little smaller than the smallest SmC* pitch (about 700 Å). In this case, if we consider that the TGBC* phase has a chance of occurring only when l_b is larger than the SmC* pitch, we can conclude that the compound studied exhibits no TGBC* phase. But this intuitive argument is probably too simple; other factors like the values of the Frank constants are known to play a decisive role in the existence of TGBC* [5, 6]. Moreover, if a TGBC* phase develops, the twist must be shared between the TGB structure and the smectic structure in the blocks. This implies that the SmC* pitch in each TGBC* block is expected to be larger than that in the low temperature SmC* phase. We conclude that, for $n=13$, X-ray scattering results seem to confirm the absence of a doubly twisted TGBC* phase in the sequence.

6. Electro-optical studies

Electro-optical properties were studied using the SSFLC configuration to evaluate spontaneous polarization, response time and tilt angle in a single set-up [39]. Commercial cells (from E.H.C., Japan) coated with indium-tin oxide and rubbed polyimide were used. The active area of the cell was 0·16 cm^2 and the thickness 3 μm. The classical set-up [42] consisted of a Eurelco 604 wave generator, a Kohn-Hite 10 W wide band amplifier and a Scientific Instruments Signal Memory Recorder, together with an Olympus BH2 microscope and Mettler FP82 hot stage.

The compounds with $n=14$ and $n=18$ were studied; the measurements were done upon cooling to facilitate the alignment. Field dependent studies showed that the saturation plateau of the polarization was reached at 5 to 10 V and the saturation field decreased with increasing temperature in the SmC* phase. In the TGBC phase the helical structure with the axis perpendicular to the cell surface was easily unwound by the electric field, also perpendicular to the cell surface, and a phase transition of TGBC to SmC* was induced by the electric field. We used square waves of field voltage 10 V (3·3 V μm^{-1}) and frequency 100 Hz for polarization and response time measurement, whereas the frequency of applied square pulse was 0·1 Hz for apparent tilt angle measurement.

The values of the spontaneous polarization (see figure 14) are quite high, as observed for many three-ring compounds. The $\mathbf{P}_s$ values have the same order for both homologues; the plateau value at lower temperature is 56 nC cm^{-2}. The response times increase also with decreasing temperature and change from 56 μs at $T=67{\cdot}5$°C to 176 μs at $T=45$°C for $n=14$, and from 100 μs at $T=67$°C to 134 μs at $T=55$°C for $n=18$ (see figure 15). The tilt angles evolve in the same way dependent on temperature (see figure 16). The values are between 17·5° and 24° for $n=14$ and between 20·5° and 24° for $n=18$.

We should note that the measurements near the TGBC–TGBA transition were quite uncertain because the helical pitch values are rather small close to the transition and the electric field (10 V) may not reach the

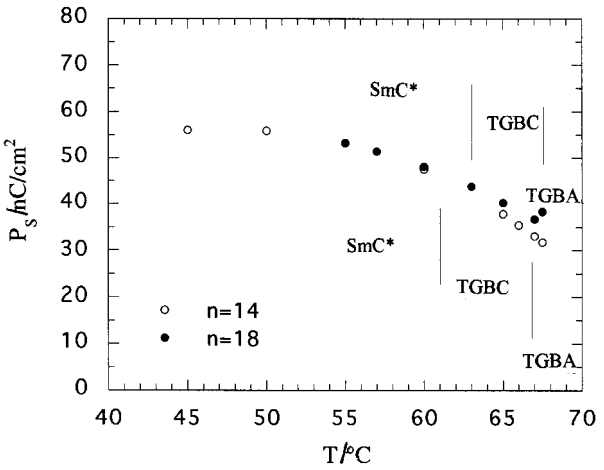

Figure 14. Spontaneous polarization versus temperature ($E=3{\cdot}3$ V μm^{-1}, $f=100$ Hz).

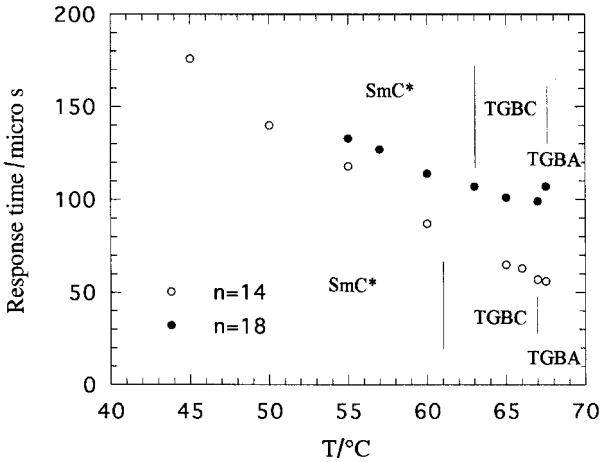

Figure 15. Response time versus temperature ($E=3{\cdot}3$ V μm^{-1}, $f=100$ Hz).

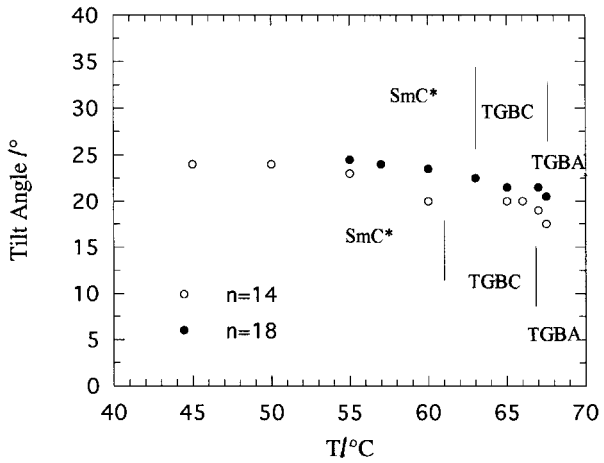

Figure 16. Tilt angle versus temperature ($E=3{\cdot}3\,\mathrm{V\,\mu m^{-1}}$, $f=0{\cdot}1\,\mathrm{Hz}$).

saturation value. An electric field-induced TGBA–SmC* transition [43] did also occur in the TGBA phase. However, a much higher field (>20–30 V) was required to unwind completely the helical structure. The electroclinic effect would occur in the TGBA phase close to the TGBC–TGBA transition as in the case of a SmC*–SmA transition [44].

7. Conclusions

We report here a series of chiral three-ring derivatives which exhibit the phase sequence Cr–SmC*–TGBC–TGBA–BPs–I. We have characterized in detail the blue phases, the TGB phases and the SmC* phase.

(1) The SmC* phase in all members of the series displays the usual structural and electro-optical properties of the ferroelectric phase. However, it has a very short helical pitch value: the smallest is about 0·06 μm which corresponds to about 20° of azimuthal angle for molecules from one layer to another.

(2) The TGBC phase exists in the members with long terminal chain length ($n=13$, 14, 16, 18, 20). The smectic layers are tilted relative to the helical axis. The TGBC phase of $n=13$ gives a commensurate χ scan with 22 blocks per pitch; unlike previously studied TGBC series, this number of blocks per pitch remains constant over the entire temperature range of TGBC. The pitch value increases with decreasing temperature, so the block size grows upon cooling.

(3) The TGBA phase is observed in all members of this series. It has very small pitch values, which are between 0·14 and 0·2 μm at the transition TGBA–BP; this very short helical pitch may be the reason for the direct transition from TGBA to blue phase. The structure of the TGBA phase is quite similar to that of other TGB materials. The smectic layers are parallel to the helical axis.

(4) Up to three blue phases are observed in the members with long chain lengths ($n=14$, 16, 18, 20). From the DSC profiles and microscopic observation, we assign BPI, BPII and BPIII to these blue phases as for normal cholesteric blue phases. Macroscopically, Kossel diagrams would be necessary to determine the crystallographic symmetry and cell parameters of these phases. We would then be able to confirm that they have the same cubic structure as normal blue phases. Microscopically, the X-ray structural analyses have demonstrated that smectic order persists (or pre-exists) in these blue phases just next to the TGBA phase. Therefore we think that they are some new kinds of blue phases: TGB blue phases. Further X-ray structural study on monocrystals of these blue phases is actually in progress. The blue phases in the members with short chain lengths ($n=13\rightarrow7$) are not detectable by microscopy because of their short helical pitches. Their assignments need to be verified. Nevertheless, the smectic-like ordering is also evident in them.

References

[1] Renn, S. R., and Lubensky, T. C., 1988, *Phys. Rev. A*, **38,** 2132.
[2] De Gennes, P. G., 1972, *Solid State Commun.*, **10,** 753.
[3] (*a*) Goodby, J. W., Waugh, M. A., Stein, S. M., Chin, E., Pindak, R., and Patel, J. S., 1989, *Nature*, **337,** 449; (*b*) 1989, *J. Am. Chem. Soc.*, **111,** 8119.
[4] Srajer, G., Pindak, R., Waugh, M. A., Goodby, J. W., and Patel, J. S., 1990, *Phys. Rev. Lett.*, **64,** 1545.
[5] Renn, S. R., and Lubensky, T. C., 1991, *Mol. Cryst. Liq. Cryst.*, **209,** 349.
[6] Renn, S. R., 1992, *Phys. Rev. A*, **45,** 953.
[7] Nguyen, H. T., Bouchta, A., Navailles, L., Barois, P., Isaert, N., Twieg, R. J., Maaroufi, A., and Destrade, C., 1992, *J. Phys. II Fr.*, **2,** 1889.
[8] Navailles, L., Barois, P., and Nguyen, H. T., 1993, *Phys. Rev. Lett.*, **71,** 545.
[9] Navailles, L., Pindak, R., Barois, P., and Nguyen, H. T., 1995, *Phys. Rev. Lett.*, **74,** 5224.
[10] Reinitzer, 1888, *Monatsh. Chem.*, **9,** 421.
[11] (*a*) Coates, D., and Gray, G. W., 1973, *Phys. Lett.*, **45A,** 115; (*b*) Armitage, D., and Price, F. P., 1976, *J. Appl. Phys.*, **47,** 2735.
[12] Stegemeyer, H., and Bergmann, K., 1980, *Liquid Crystals of One- and Two-Dimensional Order*, edited by W. Helfrich and A. Heppke (Springer), p. 161.
[13] Stegemeyer, H., Blümel, T. H., Hiltrop, K., Onusseit, H., and Porsch, F., 1986, *Liq. Cryst.*, **1,** 3.
[14] Crooker, P. P., 1989, *Liq. Cryst.*, **5,** 751.
[15] Leforestier, A., and Livolant, F., 1994, *Liq. Cryst.*, **17,** 651.

[16] Onusseit, H., and Stegemeyer, H., 1984, *Z. Naturforsch.*, **39a,** 658.
[17] Nguyen, H. T., Salleneuve, C., Babeau, A., Galvan, J. M., and Destrade, C., 1987, *Mol. Cryst. Liq. Cryst.*, **154,** 147.
[18] Li, M. H., Nguyen, H. T., and Sigaud, G., 1996, *Liq. Cryst.*, **20,** 361.
[19] Kelly, S. M., 1989, *Helv. Chim. Acta*, **72,** 594.
[20] Nabor, M. F., Nguyen, H. T., Destrade, C., Marcerou, J. P., and Twieg, R. J., 1991, *Liq. Cryst.*, **10,** 785.
[21] Austin, W. B., Bilow, N., Kelleghan, W. J., and Lau, K. S. Y., 1981, *J. Org. Chem.*, **46,** 2280.
[22] Mitsunobu, O., and Eguchi, M., 1971, *Bull. Chem. Soc. Jpn.*, **44,** 3427.
[23] Marcus, M., 1982, *Phys. Rev. A*, **25,** 2272.
[24] (*a*) Goodby, J. W., Nishiyama, I., Slaney, A. J., Booth, C. J., and Toyne, K. J., 1993, *Liq. Cryst.*, **14,** 37; (*b*) Goodby, J. W., Dunmur, D. A., and Collings, P. J., 1995, *Liq. Cryst.*, **19,** 703.
[25] Collings, P. J., 1984, *Phys. Rev. A*, **30,** 1990; 1984, *Mol. Cryst. Liq. Cryst.*, **113,** 277.
[26] Kleiman, N., Bischop, D. J., Pindak, R., and Taborek, P., 1984, *Phys. Rev. Lett.*, **53,** 2137.
[27] Thoen, J., 1988, *Phys. Rev. A*, **37,** 1754.
[28] Kutnjak, Z., Garland, C. W., Passmore, J. L., and Collings, P. J., 1995, *Phys. Rev. Lett.*, **74,** 4859.
[29] Goodby, J. W., Slaney, A. J., Booth, C. J., Nishiyama, I., Vuijk, J. D., Styring, P., and Toyne, K. J., 1994, *Mol. Cryst. Liq. Cryst.*, **243,** 231.
[30] Bouchta, A., Nguyen, H. T., Navailles, L., Barois, P., Destrade, C., Bougrioua, F., and Isaert, N., 1995, *J. Mater. Chem.*, **5,** 2079.
[31] Nguyen, H. T., Twieg, R. J., Nabor, M. F., Isaert, N., and Destrade, C., 1991, *Ferroelectrics*, **121,** 187.
[32] Bouchta, A., Nguyen, H. T., Achard, M. F., Hardouin, F., Destrade, C., Twieg, R. J., Maaroufi, A., and Isaert, N., 1992, *Liq. Cryst.*, **12,** 575.
[33] Brunet, M., and Isaert, N., 1988, *Ferroelectrics*, **84,** 25.
[34] Laux, V., Isaert, N., Nguyen, H. T., Cluzeau, P., and Destrade, C., 1996, *Ferroelectrics*, **179,** 25.
[35] Pochat, P., 1996, PhD thesis, Université de Bordeaux I, N° 1560.
[36] Navailles, L., Nguyen, H. T., Barois, P., Isaert, N., and Delord, P., 1996, *Liq. Cryst.*, **20,** 653.
[37] Faye, V., Barois, P., Nguyen, H. T., Laux, V., and Isaert, N., 1996, *New J. Chem.*, **20**.
[38] Pansu, B., Li, M. H., and Nguyen, H. T., 1997, *J. Phys. II*, **7,** 751.
[39] Clark, N. A., and Lagerwall, S. T., 1980, *Appl. Phys. Lett.*, **36,** 889.
[40] Caillé, A., 1972, *C. R. Acad. Sci.*, **B274,** 891.
[41] (*a*) Galerne, Y., 1994, *Phys. Rev. Lett.*, **72,** 1299; (*b*) Navailles, L., Barois, B., and Nguyen, H. T., 1994, *ibid.*, **72,** 1300.
[42] Dupont, L., Glogarova, M., Marcerou, J. P., Nguyen, H. T., and Destrade, C., 1991, *J. Phys. II, Fr.*, **1,** 831.
[43] Kitzerow, H. S., Slaney, A. J., and Goodby, J. W., 1996, *Ferroelectrics*, **179,** 61.
[44] Destrade, C., Payan, S., Cluzeau, P., and Nguyen, H. T., 1994, *Liq. Cryst.*, **17,** 291.